

Electronic Supplementary Information

High performance solid state asymmetric supercapacitor device based upon NiCo₂O₄ nanosheets//MnO₂ microspheres

*Syed Khalid,^a Chuanbao Cao,^{*a} Lin Wang,^a Youqi Zhu^a and Yu Wu^a*

^a Research Center of Materials Science, Beijing Institute of Technology, Beijing

100081, P. R. China

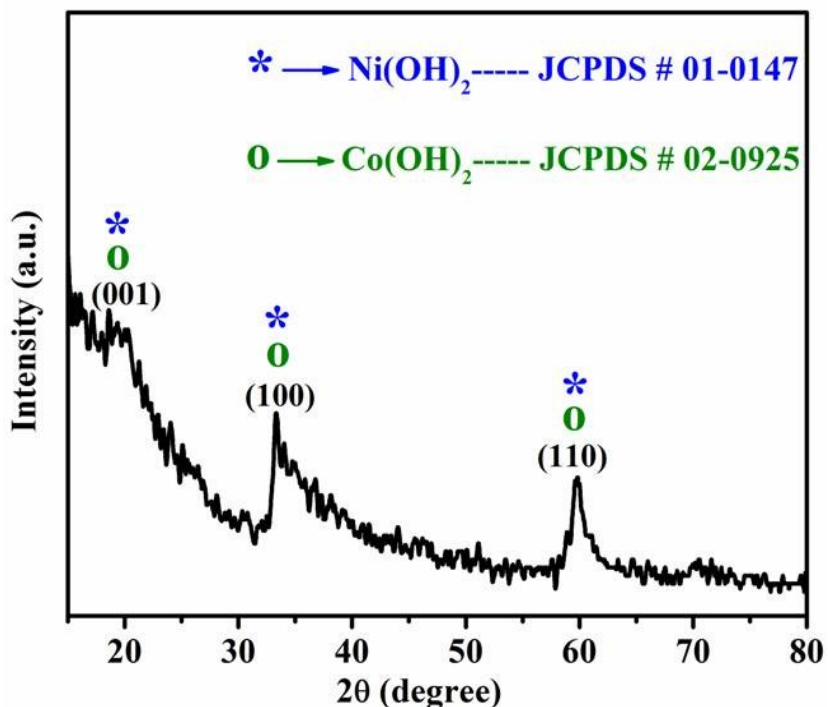


Fig. S1. XRD pattern of as-prepared precursor

Table S1. Average crystallite size calculated from XRD data of 3D hierarchical MnO_2 microspheres

Peak angle (2Θ) ($^\circ$)	Orientation	FWHM (β) ($^\circ$)	Crystallite size (nm)
36.69	(211)	0.5796	14.4
41.65	(301)	1.085	8.5
55.11	(600)	2.6188	3.5
65.95	(002)	1.073	8.8

Table S2. Average crystallite size calculated from XRD data of mesoporous layered NiCo₂O₄ nanosheets

Peak angle (2θ) (°)	Orientation	FWHM (β) (°)	Crystallite size (nm)
31.23	(220)	0.989	8.3
36.835	(311)	0.964	8.7
44.673	(400)	1.231	7.0
55.97	(422)	1.116	8.1
59.35	(511)	1.382	6.6
65.118	(440)	1.379	6.9
77.471	(533)	1.802	5.7

Table S3. Specific surface area (SSA) & pore volume (PV) comparison with reported literature

Sample	SSA (m² g⁻¹)	PV (cm³ g⁻¹)	Referenc e
3D hierarchical MnO ₂ microspheres	184.32	0.416	Our work
MnO ₂ nanosheets	157.0	-	¹
MnO ₂ nanoparticles	123.39	0.248	²

K0.17MnO ₂ nanosheets	126.31	0.344	3
MnO ₂ nanolamellas	50.3	0.135	4
MnO ₂ hollow nanospheres	167.0	-	5
MnO ₂ nanowire/Graphene	107.0	-	6
Porous MnO ₂ nanotubes	85.2	0.394	7
MnO ₂ nanoparticles	50.8	0.21	8
MnO ₂ urchin-like	76.0	0.32	9
MnO ₂ lotus shaped	145.0	-	10
MnO ₂ nanoflowers	42.45	-	11
Single-layer MnO ₂ nanosheets	74.0	-	12
Nanostructured MnO ₂ powder	90.8	0.24	13

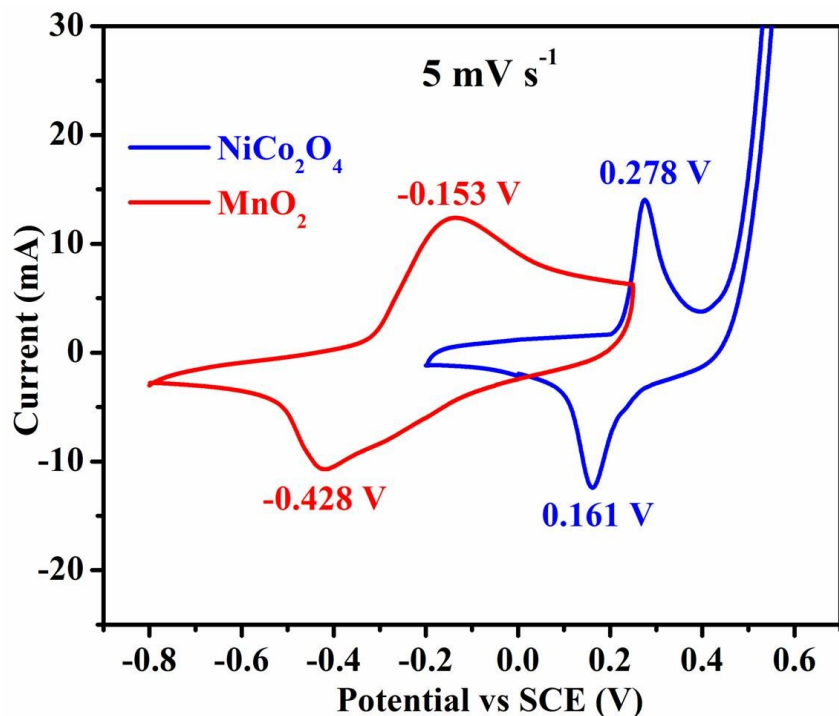


Fig. S2. CV curves of 3DHM-MnO₂ & MLNS-NiCo₂O₄ at 5 mV s⁻¹

Table S4. Areal & discharge capacities of 3DHM-MnO₂ at various scan rates

Scan rate (mV s ⁻¹)	Areal capacity (μ Ah cm ⁻²)	Discharge capacity (mAh g ⁻¹)
5	276.7	101.7
10	213.7	78.6
20	170.5	62.7
30	153.4	56.4
40	138.0	50.7
50	127.5	46.9
100	102.2	37.6

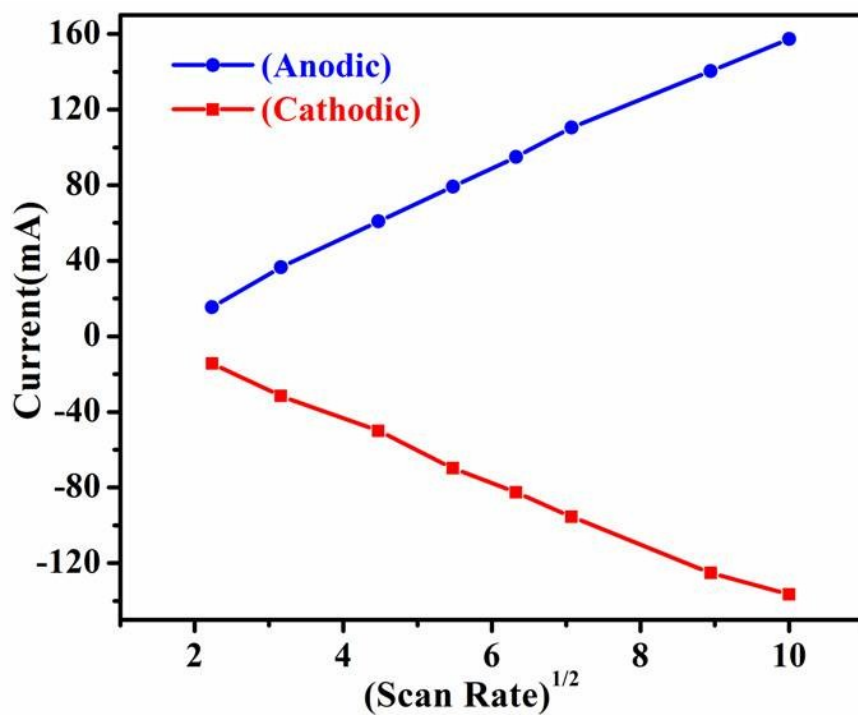


Fig. S3. Oxidation current of MLNS-NiCo₂O₄ as a function of square root of scan rate

Table S5. Areal & discharge capacities of MLNS-NiCo₂O₄ at various scan rates

Scan rate (mV s ⁻¹)	Areal capacity (μ Ah cm ⁻²)	Discharge capacity (mAh g ⁻¹)
5	344.7	221.0

10	268.0	171.8
20	223.3	143.2
30	203.6	130.5
40	187.9	120.4
50	178.0	114.1
80	156.3	100.2
100	144.4	92.6

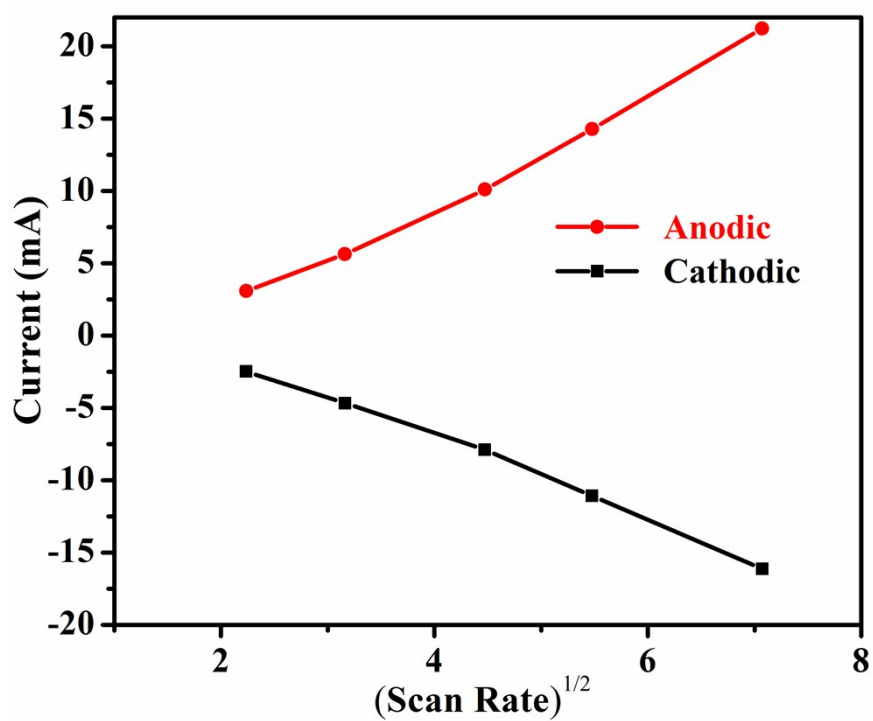


Fig. S4. Oxidation current of SSASCs device as a function of square root of scan rate

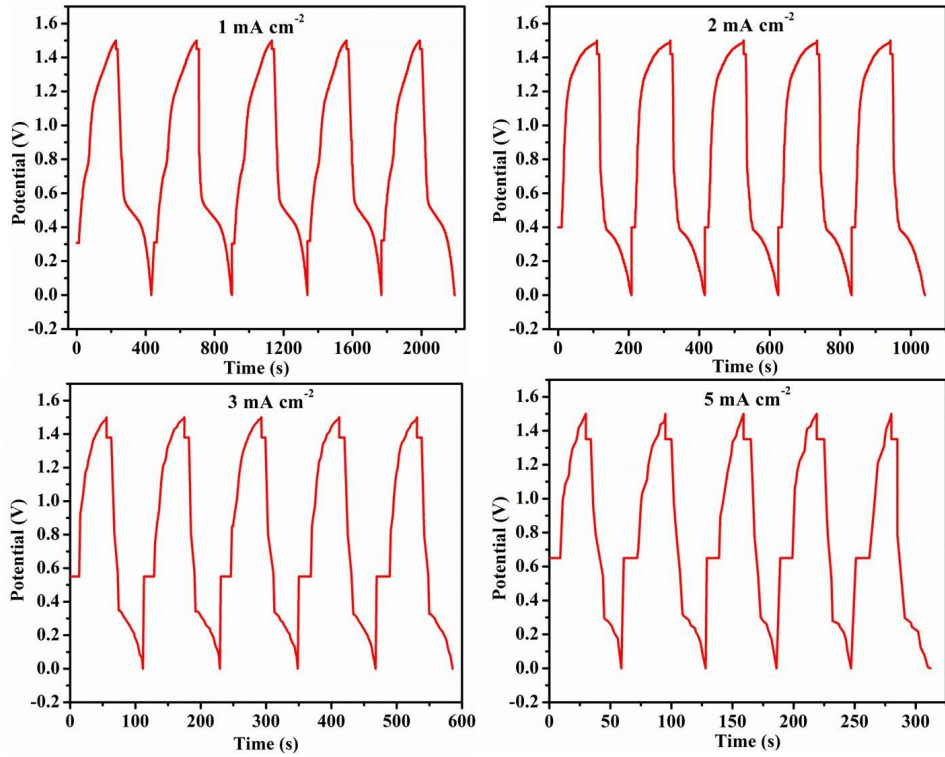


Fig. S5. CP curves for few cycles of SSASCs device at 1, 2, 3 & 5 mA cm⁻²

Table S6. Volumetric energy & power densities of SSASCs device calculated from CP curves at different current densities

Current density (mA cm⁻²)	Energy density (mW h cm⁻³)	Power density (mW cm⁻³)
1	0.715	353.6
2	0.680	468.7
3	0.583	511.3
5	0.520	625.0
8	0.388	750.0

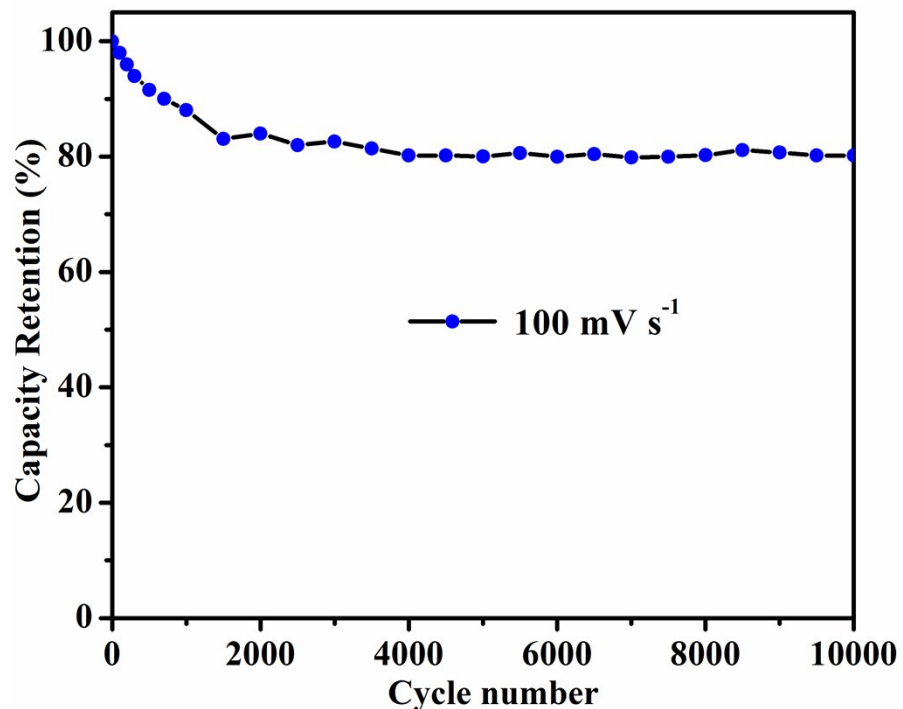


Fig. S6. Cycle performance test for 10000 cycles at a scan rate of 100 mV s^{-1} .

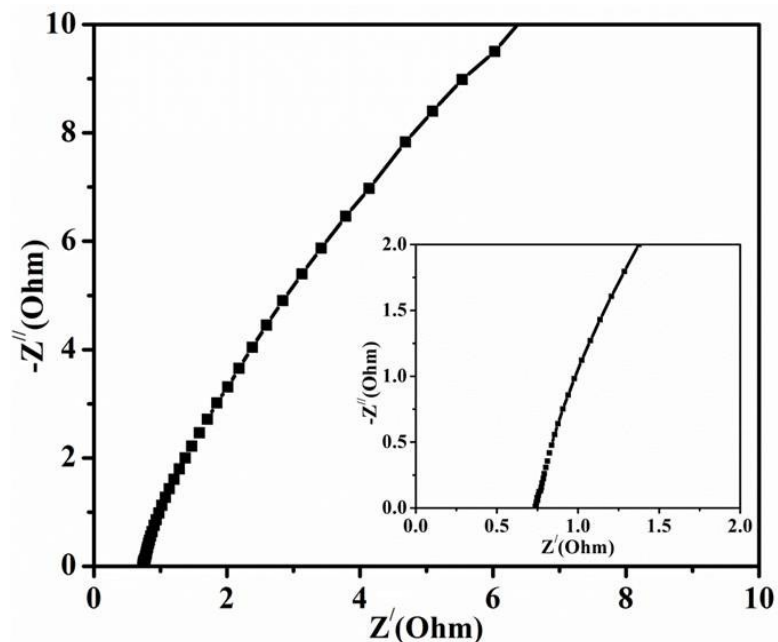


Fig. S7. Nyquist plot of as-synthesized 3DHM-MnO₂ electrode in 2.0 M KOH solution (inset: the enlarged view of high frequency region).

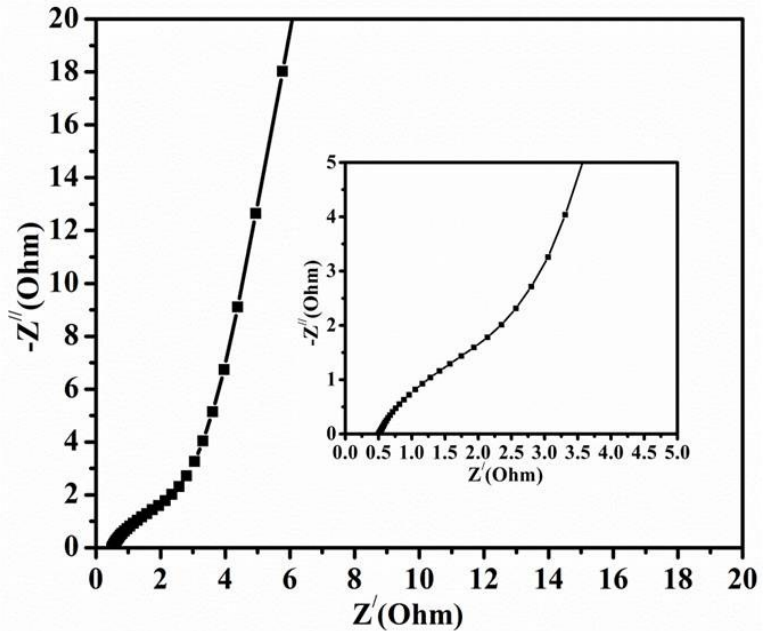


Fig. S8. Nyquist plot of as-synthesized MLNS-NiCo₂O₄ electrode in 2.0 M KOH solution (inset: the enlarged view of high frequency region).

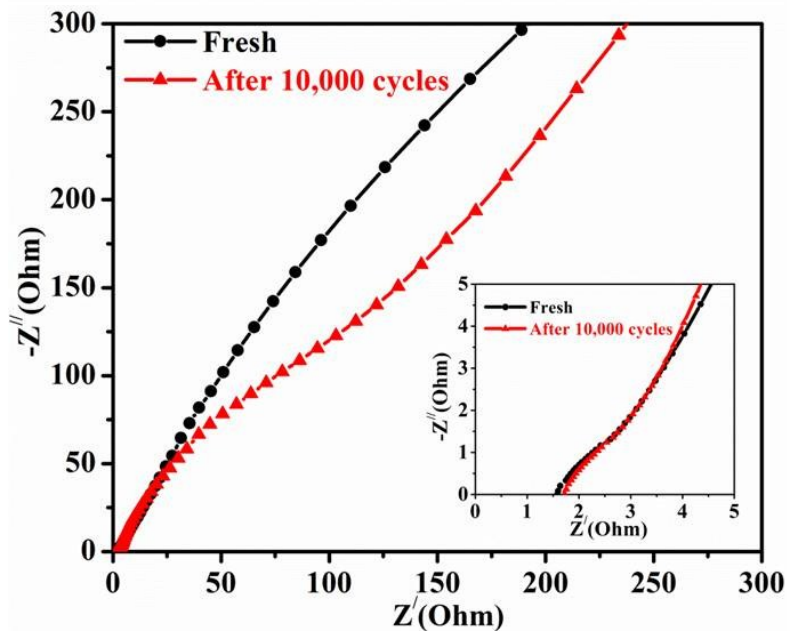


Fig. S9. Nyquist plot of fresh & 10000 CV cycles (100 mV s⁻¹) used SSASCs devices (inset: the enlarged view of high frequency region).

To investigate the intrinsic properties of the electroactive materials and SSASCs device, the EIS technique was applied to evaluate the interfacial resistance between the electrode and the electrolyte (R_s) and charge transfer resistance (R_{ct}). The Nyquist plots for the SC electrodes with 3DHM-MnO₂ and MLNS-NiCo₂O₄ as the electroactive material were shown

in Fig. S7 & S8 respectively, which presents the imaginary component (-Z'') of the impedance against the real component (Z'), demonstrating the frequency responses of the electrode/electrolyte system. The equivalent series resistance (R_s) of the SC electrodes can be estimated by the x intercept for the plots, while the charge transfer resistance at the interface of the electroactive material and the electrolyte (R_{ct}) can be evaluated by measuring the width of semicircle at the high frequency region.¹⁴⁻¹⁵ R_s values for 3DHM-MnO₂ and MLNS-NiCo₂O₄ are measured to be 0.748Ω and 0.504 Ω respectively (Fig. S7 & S8) which indicates high conductivities for both materials. It is also important to note that the width of semicircles are very small for both materials (Fig. S7 & S8) which indicates low charge transfer resistance (R_{ct}). Whereas EIS measurements of SSASCs device was carried out in fresh and after 10000 CV cycles at 100 mV s⁻¹ in two electrode configuration (Fig. S9). The values of R_s as indicated by the Nyquist plots for fresh and used SSASCs devices are 1.576 Ω & 1.717 Ω respectively (Fig. S9). The most importantly SSASCs device also exhibit very small charge transfer resistances in the fresh and even after 10000 CV cyclic test at 100 mV s⁻¹(Fig. S9).These lower R_s & R_{ct} values indicate the increased diffusion and transport pathways for electrolyte ions which are responsible for their excellent electrochemical performances.

- 1 G. Zhao, J. Li, L. Jiang, H. Dong, X. Wang and W. Hu, *Chem. Sci.*, 2012, **3**, 433-437.
- 2 S. Devaraj and N. Munichandraiah, *J. Phys. Chem. C*, 2008, **112**, 4406-4417.
- 3 J. Zhu, Q. Li, W. Bi, L. Bai, X. Zhang, J. Zhou and Y. Xie, *J. Mater. Chem. A*, 2013, **1**, 8154-8159.
- 4 S. Chen, J. Zhu and X. Wang, *ACS Nano*, 2010, **4**, 6212-6218.
- 5 J. Yue, X. Gu, L. Chen, N. Wang, X. Jiang, H. Xu, J. Yang and Y. Qian, 2014, *J. Mater. Chem. A*, **2**, 17421-17426.
- 6 Z.-S. Wu, W. Ren, D.-W. Wang, F. Li, B. Liu and H.-M. Cheng, *ACS Nano*, **4**, 2010, 5835-5842.
- 7 M. Huang, Y. Zhang, F. Li, L. Zhang, R. S. Ruoff, Z. Wen and Q. Liu, *Sci. Rep.*, 2014, **4**, 3878.
- 8 X. Zhang, W. Miao, C. Li, X. Sun, K. Wang and Y. Ma, *Mater. Res. Bull.*, 2015, **71**, 111-115.
- 9 X. Zhang, X. Sun, H. Zhang, D. Zhang and Y. Ma, *Electrochim. Acta*, 2013, **87**, 637-644.
- 10 P. Pal, S. K. Pahari, A. K. Giri, S. Pal, H. C. Bajaj and A. B. Panda, *J. Mater. Chem. A*, 2013, **1**, 10251-10258.
- 11 D. Yan, H. Zhang, S. Li, G. Zhu, Z. Wang, H. Xu and A. Yu, *J. Alloy Compd.*, 2014, **607**, 245-250.
- 12 Z. Liu, K. Xu, H. Sun and S. Yin, *Small*, 2015, **11**, 2182-2191.
- 13 L. Benhaddad, L. Makhloifi, B. Messaoudi, K. Rahmouni and H. Takenouti, *ACS Appl. Mater. Interfaces*, 2009, **1**, 424-432.
- 14 C.-W. Huang and H. Teng, *J. Electrochem. Soc.*, 2008, **155**, A739-A744.
- 15 K. Wang, P. Zhao, X. Zhou, H. Wu and Z. Wei, *J. Mater. Chem.*, 2011, **21**, 16373-16378.

